Sampled Fiber Bragg Grating spectral synthesis

L. Rodriguez-Cobo,* **A. Cobo, and J. M. Lopez-Higuera**

Photonics Engineering Group, Universidad de Cantabria
Santander, 39005, Spain

**luis.rodriguez@unican.es*

Abstract: In this paper, a technique to estimate the deformation profile of a Sampled Fiber Bragg Grating (SFBG) is proposed and experimentally verified. From the SFBG intensity reflection spectrum, any arbitrary longitudinal axis deformation profile applied to a SFBG is estimated. The synthesis algorithm combines a custom defined error metric to compare the measured and the synthetic spectra and the Particle Swarm Optimization technique to get the deformation profile. Using controlled deformation profiles, the proposed method has been successfully checked by means of simulated and experimental tests. The results obtained under different controlled cases show a remarkable repetitiveness ($< 50 \ \mu\varepsilon$) and good spatial accuracy ($< 1 \ mm$).

OCIS codes: (060.3735) Fiber Bragg gratings; (070.4790) Spectrum analysis.

References and links

1. K. Hill and G. Meltz, "Fiber Bragg grating technology fundamentals and overview," J. Lightwave Technol. **15**, 1263–1276 (1997).
2. J. Lopez-Higuera, *Handbook of Optical Fibre Sensing Technology* (John Wiley and Sons Inc, 2002).
3. Z. Zang, "Numerical analysis of optical bistability based on fiber Bragg grating cavity containing a high nonlinearity doped-fiber," Opt. Commun. **285**, 521–526 (2011).
4. Z. Zang and Y. Zhang, "Low-switching power (< 45 mw) optical bistability based on optical nonlinearity of ytterbium-doped fiber with a fiber Bragg grating pair," J. Mod. Opt. **59**, 161–165 (2012).
5. M. LeBlanc, S. Huang, M. Ohn, A. Guemes, and A. Othonos, "Distributed strain measurement based on a fiber Bragg grating and its reflection spectrum analysis," Opt. Lett. **21**, 1405–1407 (1996).
6. S. Huang, M. M. Ohn, M. LeBlanc, and R. M. Measures, "Continuous arbitrary strain profile measurements with fiber Bragg gratings," Smart Mater. Sruct. **7**, 248–256 (1998).
7. J. Azaa and M. Muriel, "Reconstructing arbitrary strain distributions within fiber gratings by timefrequency signal analysis," Opt. Lett. **25**, 698–700 (2000).
8. X. Chapeleau, P. Casari, D. Leduc, Y. Scudeller, C. Lupi, R. Ny, and C. Boisrobert, "Determination of strain distribution and temperature gradient profiles from phase measurements of embedded fiber Bragg gratings," J. Opt. A-Pure Appl. Op. **8**, 775 (2006).
9. F. Casagrande, P. Crespi, A. Grassi, A. Lulli, R. Kenny, and M. Whelan, "From the reflected spectrum to the properties of a fiber Bragg grating: a genetic algorithm approach with application to distributed strain sensing," Appl. Opt. **41**, 5238–5244 (2002).
10. C. Cheng, Y. Lo, W. Li, C. Kuo, and H. Cheng, "Estimations of fiber Bragg grating parameters and strain gauge factor using optical spectrum and strain distribution information," Appl. Opt. **46**, 4555–4562 (2007).
11. F. Teng, W. Yin, F. Wu, Z. Li, and T. Wu, "Analysis of a fiber Bragg grating sensing system with transverse uniform press by using genetic algorithm," Opto-electron. Lett. **4**, 121–125 (2008).
12. Z. Wu, Q. Qiao, F. Wu, and L. Cai, "Research on fiber Bragg grating spectral optimization with particle swarm optimization algorithm," Appl. Mech. Mater. **128**, 690–693 (2012).
13. B. Eggleton, P. Krug, L. Poladian, and F. Ouellette, "Long periodic superstructure Bragg gratings in optical fibres," Electron. Lett. **30**, 1620–1622 (1994).

14. J. Kennedy and R. Eberhart, "Particle swarm optimization," in Proceedings of International Conference on Neural Networks, ed. (IEEE, 1995), vol. 4, pp. 1942–1948.
15. M. Muriel and A. Carballar, "Internal field distributions in fiber Bragg gratings," Phot. Tech. Lett. IEEE **9**, 955–957 (1997).

1. Introduction

Nowadays, Fiber Bragg Gratings [1] are a mature technology widely used in a large set of devices for different scenarios such as sensing [2] and optical communications [3, 4], but the majority of their applications assume that no deformation or homogeneous deformations are applied to the FBG length and, consequently, that its spectral shape is maintained . However, under many real circumstances the FBG is under a non-uniform strain distribution, what modifies its spectral shape and makes it harder to obtain strain information from the spectrum.

There are several approaches that try to determine the non-uniform strain profile applied to a single FBG. In the first work based on the FBG reflection spectrum [5], the strain profile is obtained from its amplitude value, but just for monotonic strain distributions when the slope is known. Trying to reduce the a priori knowledge about the applied strain, other approach based on the Fourier Transform was proposed [6] where, using the intensity and phase of the reflection spectrum, an arbitrary strain profile was obtained. This method was very sensitive to noise and it required low FBG reflectivity (lower than 30%). A time-frequency signal analysis technique that uses the reflection spectrum intensity and phase to get the deformation profile was also proposed [7]. These works show the posibility of reconstructing any arbitrary strain profile but the suggested technique is difficult to implement with short FBG lengths. Employment of the phase measurements to get the deformation profile has also been reported [8]. This approach based on low coherence interferometry obtains any arbitrary strain profile from just two phase measurements of the FBG spectrum.

Optimization techniques have been also considered as a mean to obtain non-uniform strain distributions of a FBG. In [9], an optimization technique is applied by analyzing the intensity of a FBG reflection spectrum using a genetic algorithm. This method adjusts the coefficients of a polynomial formula that fits the deformation profile, requiring a priori knowledge of the applied deformation. On [10], an optimization algorithm is proposed to estimate some parameters of a chirped FBG under a predefined strain profile from the FBG spectrum. Genetic algorithms [11] and Particle Swarm Optimization (PSO) [12] have been also proposed to obtain the transverse strain applied to a FBG, demonstrating the capabilities of these algorithms for spectral synthesis.

In this work, a new spectral synthesis algorithm based on Particle Swarm Optimization to obtain an equivalent Sampled Fiber Bragg Grating (SFBG) longitudinal deformation profile using the reflection spectrum intensity is proposed and demonstrated. Several controlled axial deformation profiles are employed to verify both theoretical and experimentally the proposed technique, where the individual deformation of each SFBG section (<1mm) is obtained just from the intensity of the reflection spectrum without deformation restrictions. Simulations and experiments show a rather correctly deformation determination of each SFBG section under complex situations despite the model inaccuracy and fabrication imbalances.

In the next section, the theoretical model of the proposed scheme is explained. In Section 3 the optimization algorithm (PSO) is applied to an ideal SFBG model to validate the whole scheme. After the simulated model, in Section 4 the same process is applied to real spectra measured using controlled deformation profiles. The results and their discussion are shown in Section 5. Finally, a summary is presented in Section 6.

2. Theoretical model

A sampled FBG can be understood as an in-fiber grating whose axial index variation profile is modulated by a periodic sampling function of period P (Fig. 1) according to the expression [13]:

$$\Delta n(z) = s(z)a(z) \cdot A(z) \cdot e^{\left(j\frac{2\pi}{\Lambda}z + j\phi(z)\right)} + c.c. \tag{1}$$

where $s(z)$ and $a(z)$ are the sampling and the apodization functions respectively, $A(z)$ is the grating apodization profile, Λ is the FBG period and $\phi(z)$ is the phase. Currently,the period (P) of the sampling function is much larger than the period of the grating (Λ), causing a double modulation in the structure: a rapidly varying component with a period Λ and a slowly varying sampled envelope with a period P. Based on Fourier theory, the periodic sampling function of period P can be expressed as a comb function modulated by complex coefficients F_m:

$$s(z) = \sum_m F_m \cdot e^{\left(j\frac{2m\pi}{P}z\right)}. \tag{2}$$

being m the Fourier order. For each comb (m) of the Fourier equivalent function, one *ghost* grating appears on the resulting spectrum. The spectral separation between two *ghost* gratings is inversely proportional to the sampling period: $\Delta\lambda_m \propto \dfrac{1}{P}$
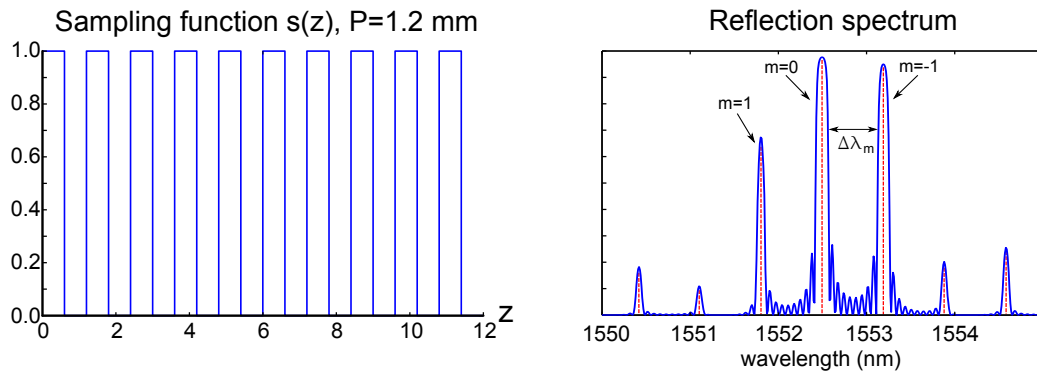

Fig. 1. No apodized ($a(z) = 1$) Sampled FBG illustration. A periodic sampling function ($s(z)$) is applied to the FBG structure creating extra reflection peaks on the reflection spectrum.

Due to its slow varying periodic structure ($P \propto 1mm$), a clear spatial division is created on the grating structure and more information (in comparison to an uniform FBG) can be obtained by analyzing the SFBG spectral response with the same span. Besides the main spectral contribution of the m=0 order, some *ghost* gratings can be also analyzed giving extra points of view of the fiber deformation structure.

The main aim of this work is to obtain the individual deformation of each of the sampled sections of the SFBG by comparing, properly, the measured spectrum to a synthetic one. The later is generated by the proposed theoretical model from a strain profile for a given SFBG. The optimization algorithm is used to adjust the deformation of each section until the synthetic spectrum matches the measured one. This challenge leads to two main goals: the assignation of a metric that compares two spectra and the optimization of a N-dimensional blind problem (being N the number of sections of the SFBG).

In order to determine the deformation profile (with the sampling period resolution), each sampled section is deformed within a fixed range. For each deformation case, the SFBG response is calculated (synthetic spectrum) and compared to the measured (desired) spectrum. For this reason, the metric to evaluate the error between the synthetic and the desired spectra and the optimization technique used to calculate the deformation of each section are very critical.

2.1. Metrics for spectral comparison

The whole synthetic spectrum challenge relies on a correct error metric for spectral comparison. Using an incorrect metric can lead the optimization algorithm to a wrong solution by assigning a lower error to a worse deformation profile. The employed error metric may also be able to manage the noise and acquisition differences of the measured spectra and the synthetic ones because the synthetic algorithm must work with real spectra. Thus, the error metric may have enough sensitivity to distinguish between two similar deformation cases but it also may deal with the noise in real data. In order to meet both requirements, some parameters of each spectrum are evaluated providing extra points of view:

- **Spectra correlation:** The correlation between the two central wavelengths of both spectra is calculated. This metric should be enough if there had not been noise and measurement errors in the spectra, consequently this value should be complemented with other parameters in a real situation.

- **Peak position:** The difference between the wavelength of the most relevant peaks of the synthetic and measured spectrum is calculated. This value can indicate an offset deformation between the two compared spectra.

- **Peak value:** The difference between the reflection value of the most relevant peaks of the synthetic and measured spectra is calculated. When a different strain profile is applied to a SFBG, the peak reflection values also change depending on the grating deformed length matching each grating period (wavelengths).

- **Peak width:** The width (measured in nm) of the most relevant peaks of the synthetic and measured spectra is calculated. This error value will penalize when the most reflective peaks are not the same in different spectra.

- **Peak ratio:** The ratio between the two most relevant peaks is calculated. The peak ratio should remain unaltered despite the intensity noise.

- **Number of peaks:** The number of peaks above a specific threshold of both spectra are also subtracted. As this parameter increases, it indicates that both spectra are in very different deformation cases.

- **Peak Kurtosis:** The Kurtosis of each of the most relevant peaks is computed in a prefixed lambda span. This value indicates the *sharpness* of a peak but it is also very noise sensitive.

All these parameters are scaled and added to get a single error metric. Depending on the measurement equipment and the present noise on the obtained data, some scale weights have to be trimmed. Getting a proper adjustment of the scale weights would offer more accurate results, but setting the weights to a very accurate target requires many controlled experiments. For the same experimental setup, these weights should be constant to evaluate all the obtained data in the same conditions.
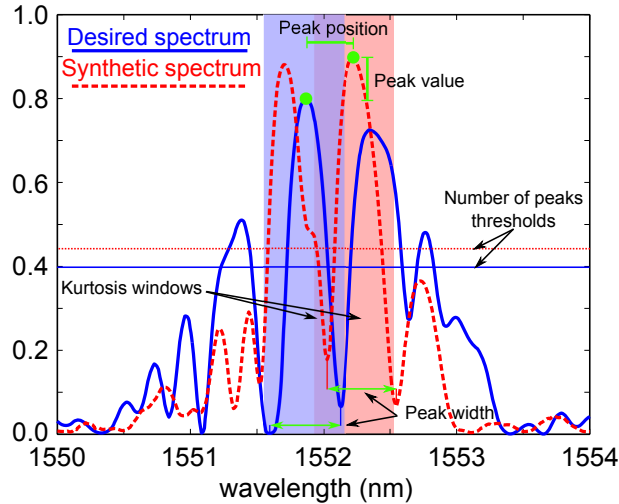
Fig. 2. Some parameters of the employed error metric are applied to two different spectra. The main peak from both spectra are just considered for drawing clarity.

In Fig. 2, a comparison between two spectra is shown. The most remarkable parameters are detailed considering just the main peak of both spectra (for drawing clarity). Besides the correlation between the central section of the desired spectrum and the synthetic one, the main peak position, peak value and peak width are computed as individual contributions to the final error value. The employed thresholds (the half value of the higher peak) to get the number of peaks of each spectra are also shown, obtaining four peaks for the desired spectrum and two for the synthetic one. The windows where the kurtosis of the most relevant peak of each spectrum is evaluated are also shown. Most of the employed metrics can be applied to a higher number of peaks, increasing the final error value with unmatched spectra.

2.2. *Optimization method: particle swarm optimization*

Once the error function between the synthetic and measured spectrum has been defined, an optimization strategy can be followed to minimize it. The target is to get a synthetic spectrum from a simulated deformed case that matches the measured spectrum obtaining the equivalent deformation profile of the measured SFBG. To obtain the equivalent deformation profile, each SFBG section is individually deformed by the optimization algorithm.

A blind optimization operation has to be performed into a N-dimensional space to get the equivalent deformation profile, where N is the number of sections of the SFBG. After some initial studies, Particle Swarm Optimization (PSO) [14] was chosen as a suitable technique to be applied in this field, given its simplicity and widespread use in several scenarios.

In a simplified way, PSO is a blind optimization algorithm that moves a population of candidate solutions (particles) within a search-space according to a prefixed rule. Each particle's best position and the swarm (collection of particles) best position are taken into account to the particle movement as well as each particle's current position and velocity. Two random values are also employed for the particle's movement, helping the algorithm to explore the search-space while the swarm is being guide to the best calculated position. The original PSO algorithm can be summarized as follows:

1. Initialize a population array of particles (SFBG strain vector) with random positions and velocities in the search space of N dimensions (number of SFBG sections).

2. Evaluate the error function for each particle (comparing the synthetic spectrum of each particle with the desired one as explained in Section 2.1).

3. Compare the latest error evaluation of the current particle with its "previous best" error value: p_{best}. If the current error value is better, then p_{best} will be updated, and p_i (previous best position) will be updated to the current location x_i.

4. Determine the particle within the swarm with the best error value (g_{best}) and assign its location to p_g.

5. Change velocity and position of each particle within the swarm according to the following expression:

$$\begin{cases} v_{id}(t+1) = w \cdot v_{id}(t) + c_1 \cdot r_1 \cdot (p_{id}(t) - x_{id}(t)) + c_1 \cdot r_1 \cdot (p_{gd}(t) - x_{id}(t)) \\ x_{id}(t+1) = x_{id}(t) + v_{id}(t+1) \end{cases} \tag{3}$$

Where w is the inertia weight, c_1 and c_2 are positive constants, typically defined as learning rates, and r_1 and r_2 are random functions in the range [0,1].

6. If the stopping condition is met then exit with the best result so far; otherwise repeat from point 2.

Each particle within the swarm is defined by its position X_i and velocity V_i within the N-dimensional search space, where:

$$\begin{cases} X_i = (x_{i1}, x_{i2}, \ldots, x_{iN}) \\ V_i = (v_{i1}, v_{i2}, \ldots, v_{iN}) \end{cases} \tag{4}$$

The position of each particle (X_i) represents a possible strain vector applied to the SFBG model and the velocity (V_i) is a vector that represents how the particle evolves within the search space. With the proposed error metric, the optimization goal is to find the deformation profile that causes the desired spectrum so, the best particle position found during the PSO run should match the physical strain profile of the SFBG. Due to the stochastic nature of the PSO, the obtained strain vector (X_p), corresponding with the best error value found in the swarm (g_{best}), may be also a local minimum of the error function. By using a high (> 100) number of starting particles should be enough to reduce the local minimum convergence. However, wrong solutions caused by a local minimum can be detected just by comparing the obtained best error value (g_{best}) to a specific threshold. If a wrong solution is detected, the PSO algorithm should be run again with a higher number of starting particles.

The PSO algorithm with the defined error metric has been tested with different deformation cases using both simulated and experimental spectra. All the performed tests are based on a $N = 5$ section SFBG with a total length of $L = 4\ mm$ and with a linear decreasing apodization profile with a decreasing factor $M = 0.25$. For each strain vector, the synthetic spectrum is calculated using the Transfer Matrix method (with $N = 5$ sections) and compared to the desired one with the defined error function. The spatial resolution of the employed structure is $P/2 = 0.8\ mm$. In the following section, the response of the algorithm to simulated spectra is analyzed under ideal and realistic situations.

3. Theoretical simulations

Some simulations have been performed by feeding artificial SFBG spectra to the PSO algorithm. These artificial spectra were simulated by applying different strain profiles to the SFBG

structure. Artificial spectrum runs have been used to check the whole optimization algorithm and to adjust the error function scale factors.

On the first tests, each section of the SBFG is uniformly deformed using different strain values for each section. This case reproduces an ideal situation where the deformation profile exactly matches the spatial resolution of the structure ($P/2 = 0.8$ mm). On the other simulated cases, the deformation value applied to each section is non-uniform, trying to reproduce a continuum strain profile. All the artificial spectra are generated using the Transfer Matrix method [15]. For the uniform deformation scenarios, the number of employed sections to compute the artificial spectrum is set to $N = 5$, matching the SBFG structure. For the non-uniform deformation cases, the number of employed sections was set to $N = 50$, having $N_s = 10$ different deformation values within each sampling section.

All the performed tests were simulated using a wavelength span of 5 nm with a resolution of 5 pm. Due to the reduced wavelength span, and also to allow an in-range convergence, the SFBG sections with null envelope ($A(z) = 0$) are initialized to a random number within the deformation values of their neighboring sections. Detecting an out-of-range deformation of the null enveloped sections could be impossible dealing with a limited wavelength span. This assumption also recreates a real situation where a particular section deformation is related to the deformation applied to its neighbors.
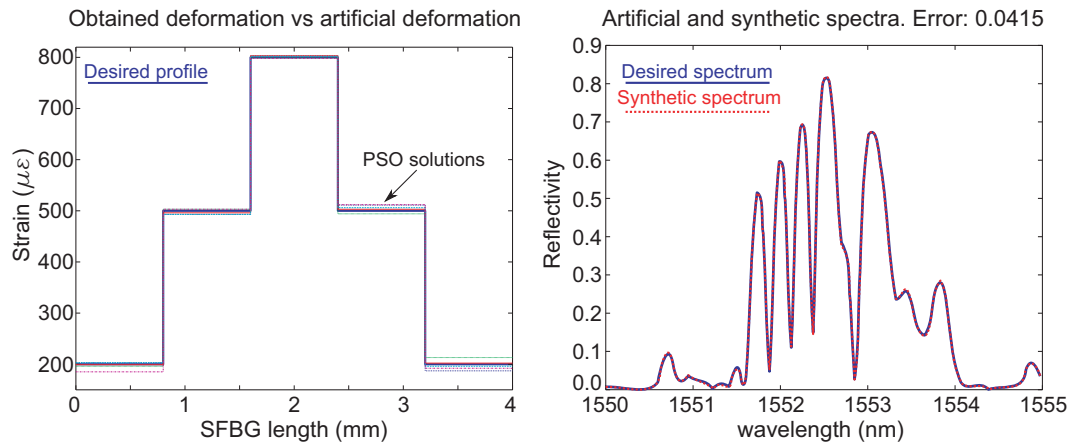

Fig. 3. Five solutions obtained by the proposed optimization algorithm compared to the reference deformation values used to generate the artificial spectrum (left) and a synthetic spectrum generated with the PSO solution compared to the artificial (desired) one (right).

In Fig. 3 (left), five strain profiles obtained with the proposed algorithm are shown against the deformation profile of the artificial spectrum. The PSO output converges to the correct strain profile employed to compute the artificial spectra. Due to the continuum range value of the algorithm outputs and to the stochastic convergence of the PSO technique, solutions considered as "correct" are distributed within a range. For this test, the achieved range which contains the correct solution is $\Delta\varepsilon = \pm15\mu\varepsilon$. On the right side (Fig. 3), the synthetic spectrum of the best achieved solution is compared to its artificial (desired) spectrum. Both spectra match each other almost perfectly, giving rise to an error value lower than 0.25 that has been considered the error stop condition. Although these tests recreate situations where the spatial deformation variations perfectly match the proposed sensing structure ($P/2 = 0.8$ mm), they are helpful to validate the algorithm resolution and repeatability.

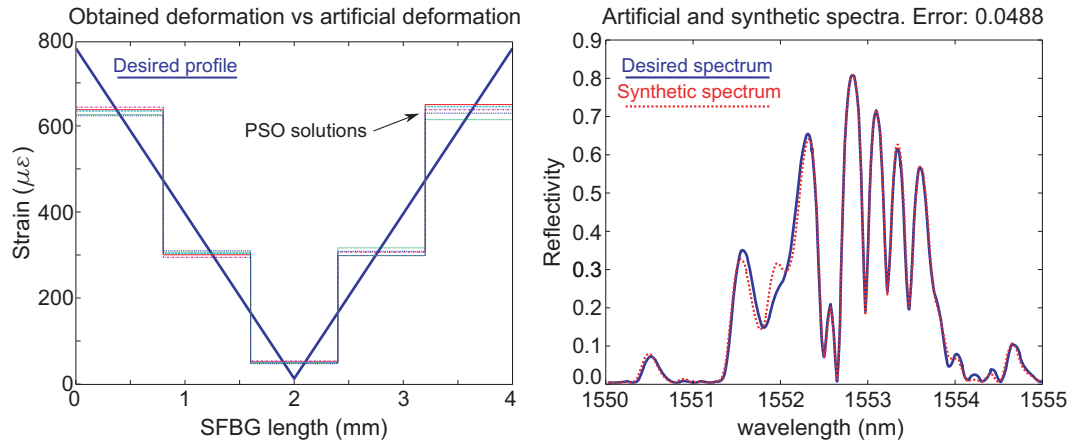A more realistic scenario is also proposed: the deformation of each sensing section is not

Fig. 4. Continuous strain profile used to compute the artificial spectrum compared to five PSO solutions (left) and a synthetic spectrum compared to the artificial one (right).

uniform along the section length ($P/2 = 0.8$ *mm*). A two-stages linear varying deformation profile is used to generate the artificial spectrum. In Fig. 4 (left), five obtained strain profiles are compared to the strain profile used to generate the artificial spectrum. As the resolution of the sensing principle is limited to the section length, the obtained strain for each section is the averaged deformation of the correspondent length. The resulting strain profiles qualitatively follow the deformation profile applied to get the artificial spectrum. In these tests, the achieved range that contains the correct solution is $\Delta\varepsilon = \pm 30\mu\varepsilon$. This range is worse than the already commented but it still is sufficiently small to be considered as highly accurate. In Fig. 4 (right), the synthetic spectrum of the best obtained solution is compared to the artificial one. The two depicted spectra are in good agreement, having a small error value (lower than the established threshold of 0.25 for simulated scenarios). The synthetic spectrum exhibits the same characteristic shape as the artificial one: two smooth peaks at lower wavelengths followed by four sharper peaks at higher wavelengths. There are slight mismatches due to the higher order spectral components of the simulated spectra. These components are more sensitive to slight mechanical deformations introduced, in this scenario, by the spatial resolution of the employed model. This second case is more realistic, thus demonstrating the good algorithm response even under non-ideal conditions.

4. Experimental demonstration

Some experimental tests were also performed using controlled SFBG deformations to validate the proposed sensing principle. A controlled strain profile is applied to a short SFBG (a few millimeters) to analyze the algorithm performance. The SFBG is embedded into a plastic block with a predesigned shape that deforms the optical fiber following a preset profile, obtaining non-uniform deformation values within the SFBG length. The short SFBG was manufactured with the same characteristics of the simulated model: $N = 5$ sections of $P/2 = 0.8$ *mm* linearly apodized with a decreasing factor of $M = 0.25$ as shown in Fig. 5. This SFBG was embedded into a epoxy resin block with a specific shape to cause a non-uniform strain profile on the SBFG. The resin block has been also mechanically simulated using Finite Element Analysis to qualitatively obtain the applied deformation profile.

The SBFG was written into a standard telecommunications optical fiber using the phase mask technique with a continuous laser emitting at 244 nm. The sampling effect was generated by
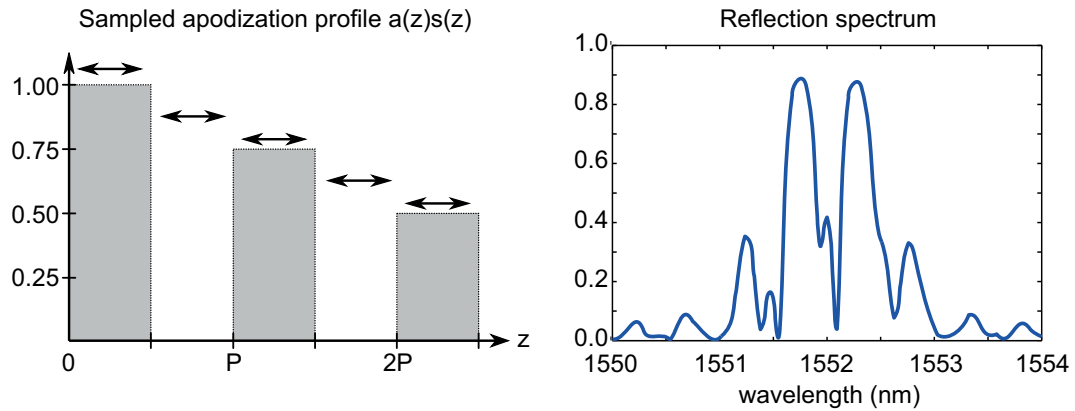
Fig. 5. Illustration of the sampled apodized SFBG profile(left) and its characteristic spectrum (right) used in the experimental demonstration.

opening and closing the laser shutter at preset locations. The apodization effect was generated by changing the recording speed during the laser scanning process: the higher the envelope, the lower the speed. To build the resin block, the FBG was aligned with a nonstick mold with the desired shape. Once the SFBG was placed into the mold, a low viscosity epoxy resin was poured into it. To build the nonstick mold, a male mold was mechanized with the desired shape in PMMA using a Computer Numerical Control (CNC) cutting machine. This male mold was covered with nonstick silicone, creating the holding mold for the epoxy resin. After the resin was poured, a vacuum stage follows to guarantee the homogeneity of the final block by removing the air bubbles. The epoxy resin was thermally cured for a few hours to obtain the final block.
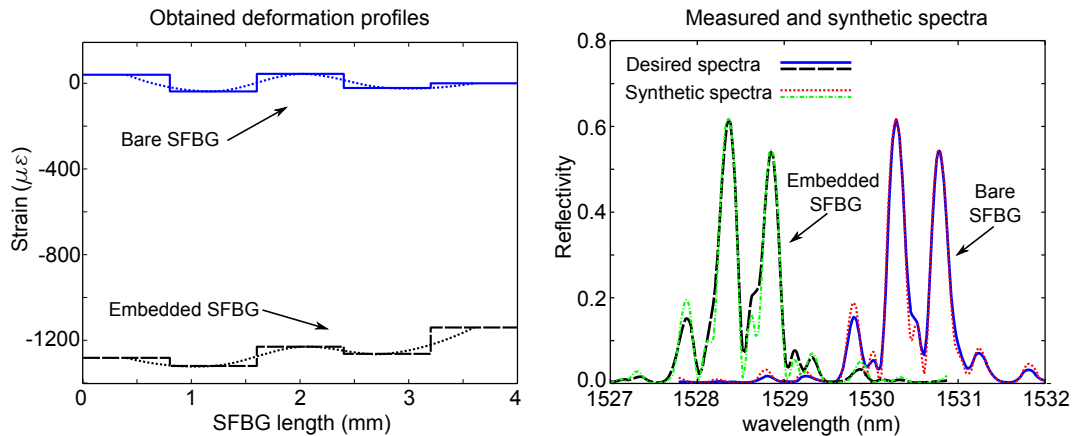

Fig. 6. Right: spectrum of the written SFBG before being embedded into the resin block (solid line) and after the embodiment (dashed line) against their synthetic spectra (thin lines). On the left: the obtained deformation profile of the residual strain and its interpolation (dotted line).

The curing process of epoxy resin introduces a residual strain to the SBFG, changing slightly its spectral shape. The small changes on the reflection spectra (Fig. 6, right) suggest a non-uniform residual strain, so a new deformation profile has to be set as a reference. The proposed

algorithm is applied to both spectra to get the residual strain profile (Fig. 6, left). The obtained deformation profile indicates that the residual strain of the final sections of the SBFG is slightly higher ($\approx 200 \; \mu\varepsilon$) than the first ones, so further deformation profiles have to be compensated using the obtained residual strain profile as a reference. This compensation step is required since the entire block is stretched, not just the written SFBG, so the reference deformation profile is the packaged one. To obtain the strain profile transfered to the SFBG by the resin block, a Finite Element Analysis (FEA) has been carried out and it is detailed in the following.

4.1. Finite element analysis

A simplified resin block model is developed by using the stress analysis suite of Autodesk Inventor (Autodesk Inc). Making highly reliable FEA models of heterogeneous pieces with absolute results can be a very complicated issue, but the generation of a qualitative deformation profile can be usually accomplished by means of a simplified model. Within this scenario, the acquisition of this qualitative profile allows to study the deformation caused to the SFBG when a load is applied.

The pierced central part of the resin block exhibits a higher sensitivity to longitudinal axis deformations, as shown in Fig. 7. The model is based on a constant thickness ($h = 0.8 \; mm$) resin block where an optical fiber is embedded in the longitudinal axis. The Young's modulus was set to 3.5 GPa for epoxy resin and 74 GPa for optical fiber silica. The employed SFBG of $L = 4 \; mm$ length is longitudinally centered within the resin block as shown in Fig. 7 with a tolerance of $\pm 0.1 \; mm$.
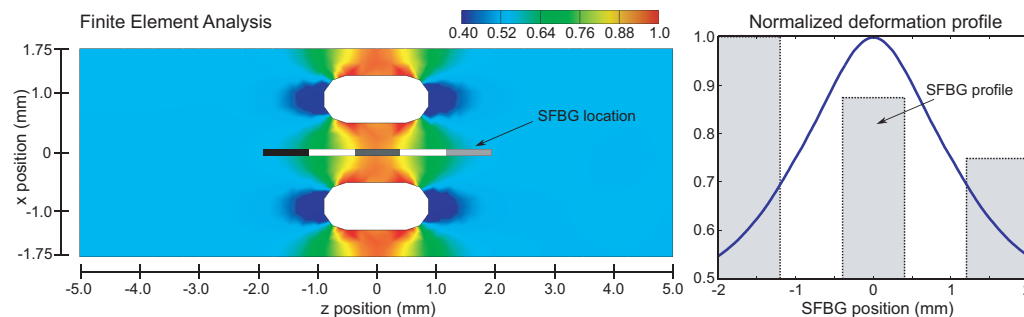

Fig. 7. Resin block dimensions and SFBG location (left). Simulated deformation profile applied to the SFBG (right)

In Fig. 7, the deformation profile applied to the optical fiber is qualitatively modeled using FEA. The pierced part of the block is more deformed than its sides when an uniform load is applied, creating a non-uniform deformation profile on the SFBG. The resin block is mounted in a mechanical setup to create the desired deformation with a controlled environment to perform the experiments discussed in the next section.

4.2. Experimental setup

The manufactured resin block is glued to two aluminum pieces separated 6 mm using cyanocrylate adhesive. The central section of the resin block is centered on the gap between the metallic pieces, leaving unglued the central block section of 6 mm. Both pieces are attached to linear micropositioners to stretch the central section of the resin block (Fig. 8). The alignment process of the aluminum pieces where the block is glued is a critical point to get an uniform load on the block. Slight misalignments can provoke an asymmetrical load to the central block section rendering useless the mechanical model. The SBFG is connected to an optical spectrum analyzer

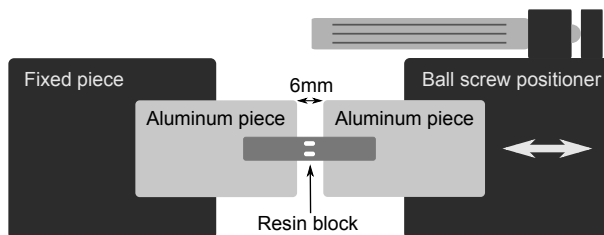(HP86140A) and to a white light source (HP83437A) through a 50/50 coupler.

Fig. 8. Experimental setup employed for loading the resin block. The block is glued to two aluminum pieces which are slightly separated using a ball screw positioner.

Once the holding pieces are perfectly aligned, the distance between the two aluminum pieces is progressively increased using the micropositioner. Reflecting spectra of the SFBG are captured for different loads (positions). These spectra are fed into the proposed algorithm to get their deformation profiles, performing $N_i = 20$ runs for each of the five captured spectra to delimit the algorithm convergence range. The stop condition for the maximum allowable error has been set to 0.75 based on previous runs. If a particular PSO run obtains a final error higher than the threshold value (less than 10% of total runs), the algorithm is executed again with a higher number of starting particles. The achieved convergence range for real spectra was $\pm 50 \, \mu\varepsilon$. The spectrum captured with the higher strain value is detailed in Fig. 9, where the obtained results for the resin block subjected to a high load are shown. On the right side, measured and synthetic spectra of the highest deformation case are presented (an increase of $\Delta L \approx 25 \, \mu m$ over $L = 6 \, mm$). Both spectra show a very good agreement (the depicted synthetic spectrum has an error metric of 0.667) exhibiting the same characteristic shape as the measured one (four sharp peaks at lower wavelengths followed by two smoother ones at higher wavelengths). However there are still small differences mainly caused to the higher order spectral components of both spectra such as the incorrect location and width of the last lobe, the value of the less reflective lobes These mismatches are created by small contributions of several factors that will be discussed in the next section. Also in Fig. 9, the deformation profile of the synthetic spectrum is compared to the normalized deformation profile simulated with FEA. The obtained profile is also compensated for the residual strain caused during the resin block. Both profiles are also interpolated for viewing purposes. The compensated profile remarkably agrees with the simulated one, thus demonstrating the correct response of the proposed algorithm.

5. Discussion

Both simulations and experimental results show a very good agreement with the applied deformations under different conditions. For achieving this remarkable agreement, the proposed algorithm has to be trimmed to better fit any particular application, so simulated tests are required to make an initial adjustment of several parameters of both error metrics and PSO algorithm. Once the algorithm parameters are set, an experimental stage follows to evaluate the whole process performance under real conditions.

The optimization algorithm is applied to two different simulated scenarios where an ideal deformation case and a more realistic one are presented. In the first deformation profile, uniform but different deformation values are applied to each of the $N = 5$ SFBG sections. Results show a perfect match between the desired and synthetic spectra with a great repeatability under this ideal environment. Once the error metric and the PSO algorithm are validated, a more realistic deformation profile where each SFBG section is deformed with a non-uniform strain profile is
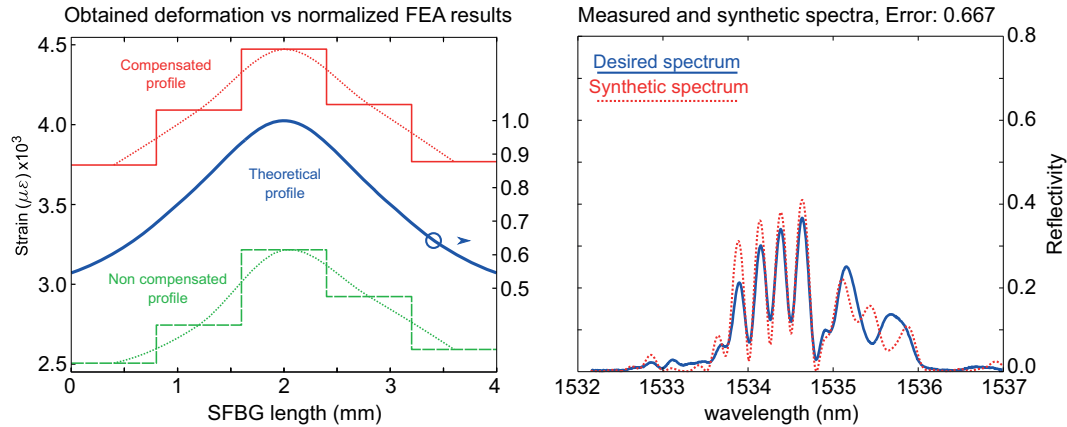
Fig. 9. Deformation profile of the measured spectrum (compensated and not) against the simulated normalized deformation (left). Measured spectrum of the SFBG under load condition compared with its synthetic one (right).

tested. The achieved results match almost perfectly the applied deformation profile proving the ability of the algorithm to work with non-uniform deformation cases.

For the experimental validation a SBFG of $L = 4\ mm$ was embedded into a resin block designed to apply a non-uniform deformation profile to the SBFG when it is stretched. The obtained deformation profiles are compared with the theoretical deformation profile obtained using FEA which is applied to the SFBG. Due to the fabrication process, a residual strain profile is created into the SFBG prior to stretching the block so the obtained deformation profiles have to be compensated with the residual strain profile. Even after the compensation, the obtained deformation profile matches the FEA simulations remarkably, having also a very good agreement between measured and synthetic spectra. Under experimental conditions the algorithm exhibits an excellent performance, but it also shows some disadvantages.

Due to the problem complexity (non-linear spectrum synthesis) and the stochastic nature of the optimization scheme (PSO), the achieved results fall within a convergence range ($\pm 50\ \mu\varepsilon$ for the experimental case). This convergence process has to be controlled by evaluating the obtained error and re-running the algorithm when it is required. In addition to the own algorithm nature, some extra factors reduce its final performance when it deals with real spectra: the simplified optical model selected to reduce the computation time does not perfectly replicate a real SFBG structure (slight misalignments during the SBFG fabrication or the apodization effect due to the laser spot width). The interpolation technique and the resolution of the Optical Spectrum Analyzer (60 pm) reduces the correlation with the synthetic spectrum (not interpolated). The limitation of the optical model, in addition to the difficulty of accurately stretching small pieces, even an incorrect gluing process may lead to less accurate results.

To deal with all these error sources, the error metric has to be carefully defined, being enough discriminant to reach the correct synthetic algorithm, but also enough permissible to deal with the optical model and mechanical errors. In order to obtain a higher accuracy in experimental runs, the error metric was re-adjusted by changing its weights slightly, demonstrating the importance of the error metric in the whole process.

All the obtained results are based on the same SFBG structure of $N = 5$ sections of $P/2 = 0.8\ mm$ with a linear apodization, but the algorithm is applicable to any SFBG structure. By increasing the number of sections (N), the computation time is also increased. All the performed test were run in a custom implementation made in Matlab (The MathWorks, Inc.) and each run

of the whole algorithm takes a few minutes. By using a more efficient implementation, this computation time can be reduced to a few seconds for each spectrum, allowing the proposed algorithm to work in quasi-on-line applications.

6. Conclusion

In this work, an optimization algorithm has been proposed to estimate any arbitrary deformation profile applied to a SFBG just from the intensity of its reflection spectrum, being its performance successfully verified with simulations and also experimentally. The proposed algorithm combines a custom defined error metric for spectral comparison and a Particle Swarm Optimization technique to get the deformation value of each individual section ($< 1 \ mm$) of the SFBG. The error metric is a critical point to lead the PSO algorithm to the right deformation profile. Simulated tests have shown the good accuracy and repetitiveness of the proposed algorithm. An experimental demonstration has been also performed by embedding a SFBG into a resin block with a particular shape. This block shape has been simulated using Finite Element Analysis to get the deformation profile and it has been compared to the achieved deformation profile. Mechanical simulations and the obtained deformation profile show an excellent agreement, demonstrating the validity of the proposed algorithm to accurately get any deformation profile dealing with any SFBG structure with a good spatial resolution, just from the reflection spectrum intensity. The proposed technique can be very useful for distributed sensing applications based on FBG technology.